

Cosmological simulations with hydrodynamics of screened scalar-tensor gravity with non-universal coupling

A. Hammami¹ and D. F. Mota¹

Institute of Theoretical Astrophysics, University of Oslo, P.O. Box 1029 Blindern, N-0315 Oslo, Norway
e-mail: amirham@astro.uio.no
e-mail: d.f.mota@astro.uio.no

December 3, 2024

ABSTRACT

Aims. In this paper we study the effects of letting the dark matter and the gas in the Universe couple to the scalar field of the symmetron model, a modified gravity theory, with varying coupling strength. We also search for a way to distinguish between universal and non-universal couplings in observations.

Methods. The research is done utilising a series of hydrodynamic, cosmological N-Body simulations, studying the resulting power spectra and galaxy halo properties such as the density and temperature profiles.

Results. Results show that in the cases of universal coupling the deviations in the bias from Λ CDM is smaller than in the cases of non-universal couplings throughout the halos. Density profile deviations can differ significantly between dark matter and gas, with the dark matter having deviations of several factors higher than the deviations in the gas. Large halos and small halos show vastly different effects from the symmetron scalar field, a direct demonstration of the screening mechanism.

Use \titlerunning to supply a shorter title and/or \authorrunning to supply a shorter list of authors.

1. Introduction

One of the most challenging problems in the field of cosmology is to understand the accelerated expansion of the late-time Universe (Riess et al. 1998). The Λ CDM model is the most accepted explanation for this expansion, and is reached by modifying General Relativity (GR) by adding a cosmological constant, dark energy, to the energy-momentum tensor.

An alternative to adding a dark energy component to GR is to modify gravity, by altering the Einstein-Hilbert Lagrangian that the Einstein tensor is derived from. Many such modified gravity theories exist (Brans & Dicke 1961; de Felice & Tsujikawa 2010; Sotiriou 2006; Clifton et al. 2012; Boehmer & Mota 2008) and several have previously been studied by the authors (Brax et al. 2013; Barreira et al. 2013; Li et al. 2011; Li et al. 2012; Davis et al. 2012; Barrow & Mota 2003; Mota et al. 2008; Puchwein et al. 2013; Winther et al. 2012). These theories are often implemented by introducing a scalar field to the Einstein tensor that couples to the matter component of the Universe. This scalar field gives rise to fifth force, an additional gravitational force, that according to laboratory experiments (Hoyle et al. 2004; Dimopoulos et al. 2007) and solar system gravity probes (Bertotti et al. 2003; Will 2014) is negligible at solar system scales and below.

Assuming that this fifth force acts on larger scales than the solar system, then some mechanism is needed to negate the fifth force on solar system scales. One way to achieve this is to utilise one of the screening mechanisms found in the literature (Khouri 2010; Brax et al. 2012; Hinterbichler & Khouri 2010; Khouri & Weltman 2004; Vainshtein 1972; Koivisto et al. 2012) where the fifth force is screened based on a series of different criteria. In this paper we will study

the symmetron model (Hinterbichler & Khouri 2010) where the fifth force is screened in regions of high density.

With these modified gravity theories comes the challenge of finding methods for testing them against observations (Terukina et al. 2014; Wilcox et al. 2015). Theorists in the past have mainly been using predictions from dark matter (DM) only models and simulations, due to the simplistic nature of the dark matter, when constraining modified gravity theories. Using dark matter only models can be justified by the matter composition of the Universe, 84.4% dark matter and 15.6% baryonic matter according to the Planck Collaboration et al. (2015). However, astronomers observe the electromagnetic spectrum emitted from the baryonic components of the Universe, leaving the community with a disconnect between theories and observables.

Introducing the concept of a bias between the dark matter and baryonic components is one way to rectify this disconnect. The bias assumes that the behaviour of the two components are the same, but that the strength or amplitude of the behaviour might be different. The community generally assumes that the bias of the standard model Λ CDM is equal to one, justifying that studying the Universe and comparing the observations to dark matter only simulations is valid. However, if the bias is not unity researchers might greatly underestimate or overestimate their findings.

Recent work (Schaller et al. 2015) has made progress in studying the differences between galaxies (gas) and dark matter in the Λ CDM model.

In our previous work (Hammami et al. 2015) we studied the effects of adding a hydrodynamic gas to an existing N-body code with the symmetron model implemented (Llinares et al. 2014), with the assumption that the scalar field would couple to the gas and the dark matter with a universal coupling. There are, however, no justifications for

assuming that the dark matter and gas has the same coupling to the scalar field, however, several known particles such as neutrinos and baryons do not interact in the same manner with electromagnetic forces, it therefore stands to reason that it is worthwhile to study the effects of having a non-universal coupling between the scalar field and the matter components.

In this paper we will study the density- and temperature profiles and power-spectra for dark matter and gas for the symmetron models, with different values for the coupling strength. The paper starts with an introduction to the symmetron model in Section 2, followed by a very brief section on the simulation parameters in Section 3, presenting and discussing the power spectra in Section 4 and the density- and temperature profiles in Section 5, finishing with conclusions in Section 6.

2. The symmetron model

Introduced by Hinterbichler & Khoury (2010) the symmetron model is a scalar theory of gravity using a symmetric potential, where the the action (Sotiriou 2006; Fujii & Maeda 2003) is

$$S = \int d^4x \sqrt{-g} \left[\frac{R}{2} M_{pl}^2 - \frac{1}{2} \partial^i \psi \partial_i \psi - V(\psi) \right] + S_m(\tilde{g}_{\mu\nu}, \tilde{\Psi}_i), \quad (1)$$

where ψ is the scalar field¹, R is the Ricci scalar and $g = |g_{\mu\nu}|$ in the Einstein frame, which can be converted to the Jordan frame by

$$\tilde{g}_{\mu\nu} = A^2(\psi) g_{\mu\nu}. \quad (2)$$

The conformal factor satisfy $A \simeq 1$ for the symmetron model and we will use this approximation throughout. For more on these frames and the transformations between them and possible errors see Faraoni et al. (1999) and Brown & Hammami (2012).

To preserve the behaviour of gravity, as described by GR, at the solar system scale (a region of high density) the symmetron model utilises a screening mechanism that triggers based on a set density value ρ_{assb} . In regions of low density the symmetron would produce a modification of order one on the gravity. To do this the potential in the action above is defined to be symmetric like

$$V(\psi) = V_0 - \frac{1}{2} \mu^2 \psi^2 + \frac{1}{4} \lambda \psi^4, \quad (3)$$

where ψ is the scalar field, μ is a mass scale and λ a dimensionless parameter. Likewise, the coupling factor is also symmetric,

$$A(\psi) = 1 + \frac{1}{2} \left(\frac{\psi}{M} \right)^2,$$

with M being another mass scale.

¹ We only study the quasi-static limit (Llinares & Mota 2013; Noller et al. 2014) of the scalar field, where time-derivatives are ignored.

To find the stress energy tensor for the symmetron model we vary the action with respect to the metric

$$\begin{aligned} T_{\mu\nu} &= A(\psi) T_{\mu\nu}^{(m)} + T_{\mu\nu}^{(\psi)} \\ &= A(\psi) [(P + \rho) u_\mu u_\nu + P g_{\mu\nu}] \\ &\quad + \nabla_\mu \psi \nabla_\nu \psi - g_{\mu\nu} \left(\frac{1}{2} \partial^i \psi \partial_i \psi + V(\psi) \right). \end{aligned} \quad (4)$$

Note that the scalar field component of the stress energy tensor is not covariantly conserved,

$$\nabla^\nu T_{\mu\nu}^{(\psi)} \neq 0$$

while the total stress energy tensor is (Misner et al. 1973)

$$\nabla^\nu T_{\mu\nu} = 0. \quad (5)$$

The equation of motion for the scalar field is found by varying the action again, this time with respect to the scalar field,

$$\square \psi = V'(\psi) - A'(\psi) T^{(m)}, \quad (6)$$

where $T^{(m)}$ is the trace of the stress energy tensor $T^{(m)} = g^{\mu\nu} T_{\mu\nu}^{(m)}$.

The right hand side of Eq. (6) can be recognised as an effective potential, using Eq. (4) this is

$$V_{\text{eff}}(\psi) = V_0 + \frac{1}{2} \left(\frac{\rho_m}{M^2} - \mu^2 \right) \psi^2 + \frac{1}{4} \lambda \psi^4. \quad (7)$$

With this potential the scalar field goes to zero in regions of high density, $\rho_m \gg M^2 \mu^2$, while in regions of low density it reaches a minimum of $\psi_0 = \pm \mu \sqrt{\frac{1}{\lambda}}$. The addition to gravity, the fifth force, scales with the value of the scalar field, and we see from this that it will be suppressed in regions of high density.

Redefining the free parameters μ , M and λ to β , λ_0 and a_{SSB} to a set of parameters that are more physical intuitive as described in Winther et al. (2012):

$$\beta = \frac{M_{pl} \psi_0}{M^2}, \quad (8)$$

$$a_{SSB}^3 = \frac{3H_0^2 \Omega_m M_{pl}^2}{M^2 \mu^2}, \quad (9)$$

$$\lambda_0^2 = \frac{1}{2\mu^2}. \quad (10)$$

The relative strength of the fifth-force to the gravitational force is represented by β , the moment of symmetry breaking is represented by the expansion factor $a_{SSB} = \Omega_{m0} \rho_{c0} a_{SSB}^{-3}$, and the range of the fifth-force is represented by λ_0 in units of Mpc/h.

A dimensionless scalar field χ is defined as

$$\tilde{\psi} \equiv \psi_0 \chi, \quad (11)$$

with an equation of motion, in the quasi-static limit (Llinares et al. 2014)², is

$$\nabla^2 \chi = \frac{a^2}{2\lambda_0} \left[\left(\frac{a_{SSB}}{a} \right)^3 \frac{\rho_m}{\bar{\rho}_m} + \chi^3 - \chi \right]. \quad (12)$$

² Simulations beyond the static limit were presented in Llinares & Mota (2013, 2014), finding only sub-percent differences between the static and non-static solutions.

The equation of motion for the position x of the dark matter N-Body particles has been derived from Eq. (1) in Llinares et al. (2014) and take the form

$$\ddot{x} + 2H\dot{x} + \frac{1}{a^2}\nabla\Phi + \frac{1}{a^2}\frac{A'(\psi)}{A(\psi)} = 0. \quad (13)$$

The fluid equations for the symmetron model is a special case of the general fluid equations for a scalar-tensor theory. By using the action Eq. (1), stress-energy tensor Eq. (4), conservation law Eq. (5) and the choice of working in the Newtonian Gauge,

$$ds^2 = -(1 + 2\Phi)dt^2 + a^2(1 - 2\Phi)\delta_{ij}dx^i dx^j, \quad (14)$$

the fluid equations are derived,

$$\frac{\partial\rho}{\partial t} + \nabla(v\rho) + 3H\rho = 0, \quad (15)$$

$$a^2(P + \rho)\left[Hv + \frac{\partial v}{\partial t} + (v \cdot \nabla)v + \frac{1}{a^2}\nabla\Phi\right] \quad (16)$$

$$+ \nabla P + \frac{A'(\psi)}{A(\psi)}\rho\nabla\psi = 0,$$

$$\frac{\partial E}{\partial t} + 2HE + \frac{P}{\rho} \cdot \nabla v = -(v \cdot \nabla)\Phi - \frac{A'(\psi)}{A(\psi)}(v \cdot \nabla)\psi. \quad (17)$$

To remove explicit dependencies on a and H from the equations above we follow Martel & Shapiro (1998) and convert to super-comoving coordinates, represented by a tilde,

$$d\tilde{t} = a^{-2}dt, \quad \tilde{\rho} = a^3\rho, \quad \tilde{v} = a^2v, \quad (18)$$

$$\tilde{\psi} = a\psi, \quad \tilde{P} = a^5P, \quad \tilde{\Phi} = a^2\Phi, \quad \tilde{E} = a^2E. \quad (19)$$

By excluding terms of second order and assuming static pressure, the field Eqs. (15 - 17) change to

$$\frac{\partial\tilde{\rho}}{\partial\tilde{t}} + \nabla(\tilde{v}\tilde{\rho}) = 0, \quad (20)$$

$$\frac{\partial\tilde{v}}{\partial\tilde{t}} + (\tilde{v} \cdot \nabla)\tilde{v} = -\frac{1}{\tilde{\rho}}\nabla\tilde{P} - \nabla\tilde{\Phi} - \frac{A'(\tilde{\psi})}{A(\tilde{\psi})}\nabla\tilde{\psi}, \quad (21)$$

$$\frac{\partial\tilde{E}}{\partial\tilde{t}} + \tilde{v} \cdot \nabla\tilde{E} + \frac{\tilde{P}}{\tilde{\rho}} \cdot \nabla\tilde{v} = -(\tilde{v} \cdot \nabla)\tilde{\Phi} - \frac{A'(\tilde{\psi})}{A(\tilde{\psi})}\tilde{v} \cdot \nabla\tilde{\psi}, \quad (22)$$

With this the symmetron model version of the fifth-force is

$$F_\psi = \frac{A'(\tilde{\psi})}{A(\tilde{\psi})}\nabla\tilde{\psi} = \frac{\tilde{\psi}}{M^2}\nabla\tilde{\psi} \\ = 6\Omega_m H_0^2 \frac{(\beta\lambda_0)^2}{a_{\text{SSB}}^3}\chi\nabla\chi. \quad (23)$$

For more on the symmetron model the reader is referred to Hinterbichler & Khoury (2010).

3. Parameters

The coupling factor defined above is split into two new coupling factors,

$$\beta \rightarrow \begin{cases} \beta_{DM} \\ \beta_{gas} \end{cases}, \quad (24)$$

Table 1. Coupling factor combinations explored in this paper.

Configuration	β_{DM}	β_{gas}
DM1G1	1.0	1.0
10G10	10.0	10.0
DM0.1G0.1	0.1	0.1
DM10G1	10.0	1.0
DM1G10	1.0	10.0
DM0.1G1	0.1	1.0
DM1G0.1	1.0	0.1

which replaces the coupling factor in the dark matter and the fluid equations respectively.

In order to study the effect we choose couplings of varying orders of magnitude³, our chosen configurations are shown in Table 1.

The simulations were run using 1024 cores, 256³ dark matter particles, with a box width of 256 Mpc/h and six levels of refinements. The background cosmology is a standard Λ CDM background with $h = 0.65$, $\Omega_\Lambda = 0.65$, $\Omega_m = 0.35$ and $\Omega_b = 0.05$. The chosen symmetron model has $a_{\text{SSB}} = 0.33$ and $\lambda_0 = 1$ Mpc/h.

Due to the use of the extremely coupled models a set of convergence tests were run, to verify that the errors induced by the extreme coupling were not too extensive. The tests showed that the code handled the extreme models well for the most part, however, that for the power spectra there were slight errors at the smallest scales $k > 4$ Mpc/h and for the halo profiles at radius above $R > 3R_{200c}$. These errors were not significantly large, but we still urge the reader to take the extreme models with a grain of salt in these regions.

4. Power spectra

Using the open POWMES code (Colombi & Novikov 2011) we compute the power spectra for both dark matter and gas. To calculate the gas power spectrum we treat each cell as a particle with a mass, defined as

$$m = \rho V_{\text{cell}} \quad (25)$$

where ρ and V_{cell} is the gas density and volume of the cell respectively.

In Fig. 1 we present the power spectra for all our models, and the deviations of these power spectra from Λ CDM, for both the dark matter and gas components.

At the large scale range of the power spectra, $k < 1$ Mpc/h, the extreme dark matter models (10G10 and DM10G1) show stronger effects of the scalar field in the dark matter power spectra than in the gas power spectra. This is due the power spectra of a component being most sensitive to changes to that said component. The smaller

³ The extreme couplings with $\beta = 10$ can induce accelerations upwards of $F_\psi = 200F_{GR}$. Accelerations of this kind can result in relativistic velocities, requiring a relativistic set of equations to properly describe the systems. Luckily, none of the models in this paper induced relativistic velocities, the fastest dark matter particle in our simulations reached a speed of $v_{max} = 0.033c$ for the 10G10 model, barely a factor of 2 higher than the fastest dark matter particle in the Λ CDM model with $v_{max} = 0.016c$. With this we choose to continue with the extreme models in order to probe a wide range of various couplings.

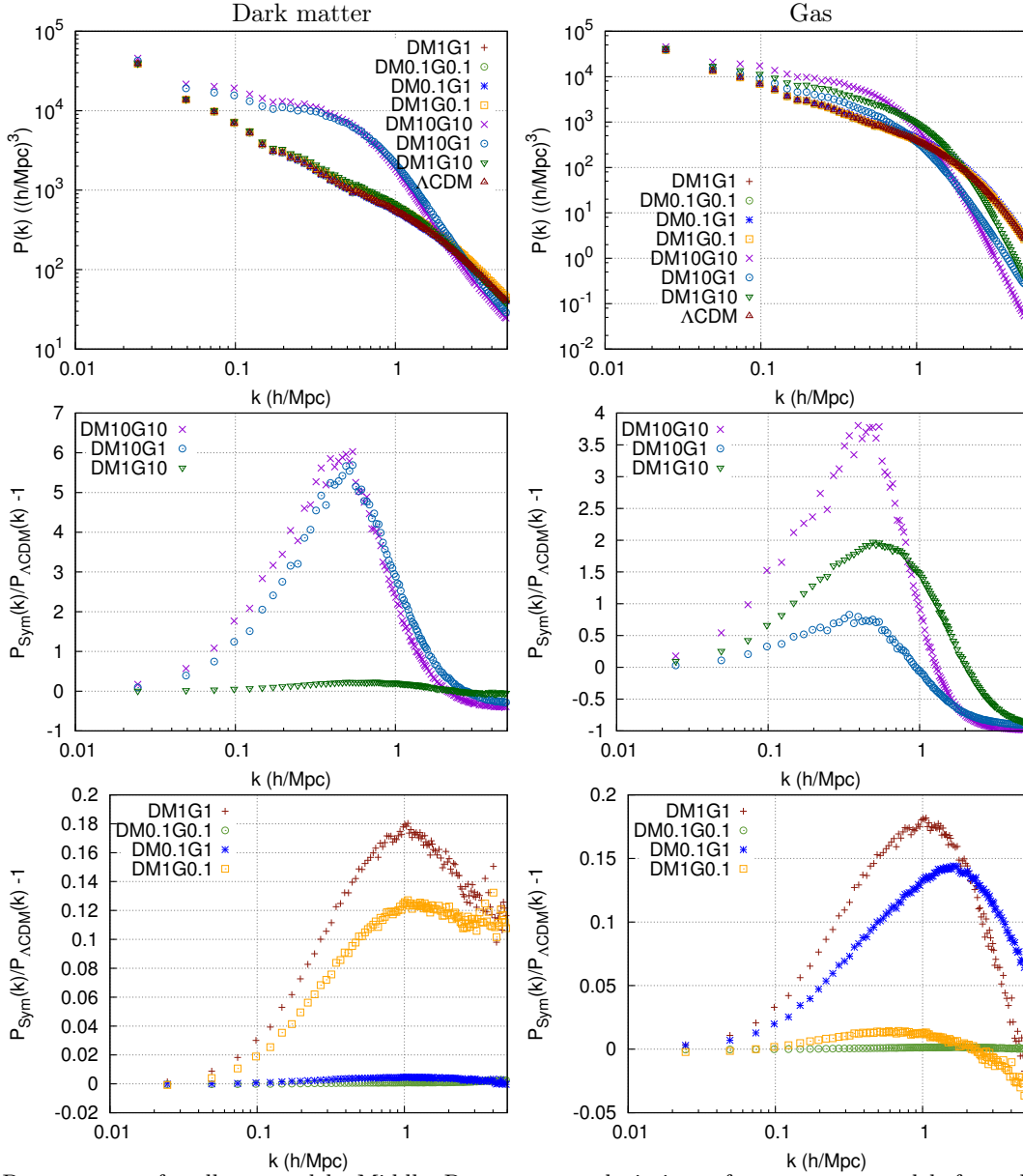


Fig. 1. Top: Power spectra for all our models. Middle: Power spectra deviations of our extreme models from the Λ CDM model. Bottom: Power spectra deviations for the remaining models. Left column show the dark matter component, while the right column show the gas component.

differences between the various models in the gas spectra is due to the simulation being strongly dominated by dark matter compared to the gas, so that the extreme gas model (DM1G10) is being suppressed by the dark matter, which also accounts for DM1G10 not being clearly distinguishable in the dark matter spectra.

On the smaller scales, $k > 1$ Mpc/h, the variations between the models is most noticeable in the gas spectra, as is to be expected as the baryonic processes are strong at the smaller scales.

Overall we see a clear example of big deviations in the dark matter power spectra does not mean big deviations in the gas power spectra.

4.1. Power spectra deviations

The main difference between 10G10 and DM10G1 in the dark matter power spectra deviations is that the latter is

shifted slightly towards smaller scales and have a slightly smaller amplitude. The addition of the extremely coupled gas increases clustering on larger scales, while decreasing it on smaller scales.

The gas spectra deviations show that the spectra is greatly influenced by both the dark matter and the gas, this is evident by 10G10 having the strongest deviations, while the second and third largest deviations come from DM1G10 and DM10G1 respectively. The effect of the dark matter on the gas spectra is much stronger than the effect of the gas on the dark matter spectra, a consequence of the dark matter dominance.

DM1G1 and DM1G0.1 show that having a minimally coupled gas reduces the amplitude of the power spectra in the range $k \in [0.1, 3)$, with the largest difference from DM1G1 at $k \sim 1$ Mpc/h. However, at the smallest scales these models end up with the same amplitude, indicating

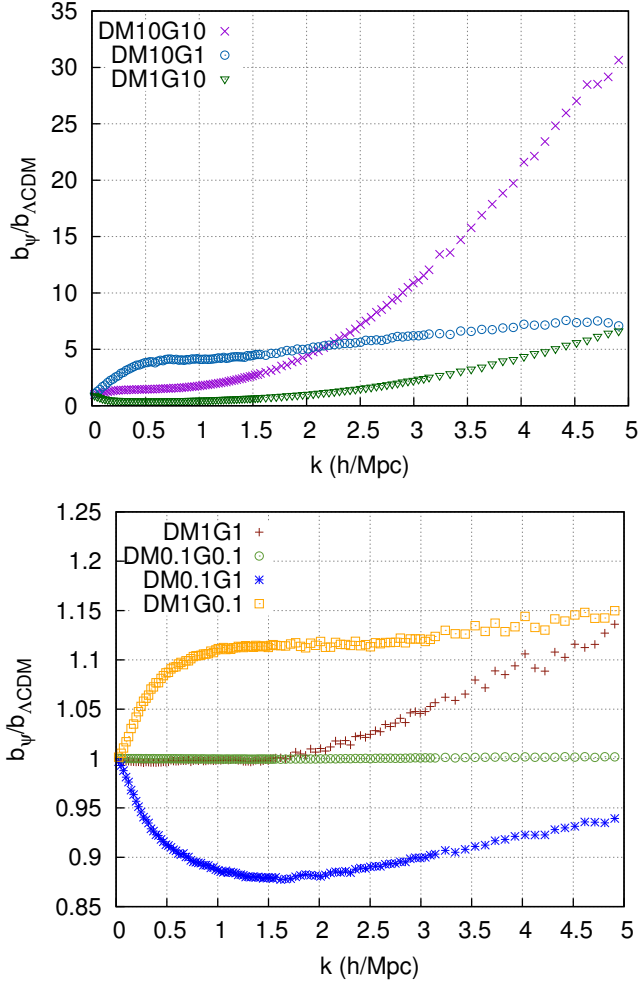


Fig. 2. Deviation of the bias from the Λ CDM bias for our various models. The top image show the extreme models, the bottom image the remaining models.

that at this point the gas coupling is irrelevant for the dark matter spectra.

The models DM0.1G0.1 and DM0.1G1 reveal that the gas does have an impact on the dark matter spectra although not significantly, the same very minor effect was also evident when comparing DM1G10 to 10G10 and DM10G1.

The gas spectra is more susceptible to changes to the dark matter coupling, however it is still most dependent on the gas coupling, as demonstrated by the increasing amplitude as DM10G1 < DM1G10 < 10G10. Note that all the models with an extreme coupling has a very low amplitude at small scales, and at the very smallest scales they all end up at more or less the same value regardless of whether the coupling is universal or not. The same effect is seen when comparing DM1G1 to DM0.1G1.

4.2. Bias

The bias is defined as the ratio between the gas power spectrum and the dark matter power spectrum,

$$b = \frac{P_{\text{DM}}}{P_{\text{gas}}}, \quad (26)$$

and is shown in Fig. 2 In the large scale region, $k < 1$ Mpc/h, the DM10G1 model has a much higher bias than

the other models, while DM1G10 has the exact opposite behaviour of having a lower bias. 10G10 behaves as a medium between these two models.

On smaller scales these models start to grow larger than the Λ CDM bias. Bias deviations in the smaller, non-linear, scales is strongly correlated with the gas coupling, while also dependent on the coupling to the dark matter. 10G10 reveal that the components compound the effect of the deviations so that the 10G10 deviation is larger than the sum of the DM10G1 and DM1G10 deviations.

DM0.1G0.1 exhibit almost no deviations from Λ CDM, as is to be expected. In the final models the behaviour of the bias deviations act in extremely different manners depending on what components are strongly coupled.

For DM1G0.1 we see that the bias deviations sky-rockets at the large, non-linear scales until it reaches a more or less constant value that is increasing slightly from $k \sim 1$ Mpc/h and out. The DM0.1G1 model has an exact opposite behaviour at the large, non-linear scales. Similar to the extreme models DM1G1 acts as a medium between the other two models at the large scales, and then eventually starts to increase to much more than the sum of the respective deviations.

Note that the power spectrum bias at larger scales show that models with a universal coupling has less deviations from the Λ CDM model than the models with a non-universal coupling.

For observational astronomers the implications of this behaviour is that if the bias deviations are greater than unity, $b_{\psi} > b_{\Lambda\text{CDM}}$, then researchers who infer dark matter properties from baryonic physics features will make predictions with too high values of the power spectrum. The opposite is true if the bias deviations are less than unity, $b_{\psi} < b_{\Lambda\text{CDM}}$.

5. Halo profiles

In this section, we present density- and temperature profiles for multiple halos identified by using the the Rockstar code developed by Behroozi et al. (2013).

Two groups of halos are selected, small halos with mass in the range $[5 \times 10^{11} h^{-1} M_{\odot}, 1 \times 10^{12} h^{-1} M_{\odot})$ and massive halos with mass in the range $[1 \times 10^{14} h^{-1} M_{\odot}, 5 \times 10^{14} h^{-1} M_{\odot})$. The small halos have a relatively low density so that the halos should be mostly non-screened from the scalar field, while the large halos have a higher density and should be mostly screened from the scalar field.

In previous works (Hammami et al. 2015; Llinares et al. 2014) the halos that had not yet reached a relaxed state were filtered out by following the methods described in Neto et al. (2007) and Shaw et al. (2006). The method used relations between the kinetic- and potential energy and the surface pressure to determine if a halo was relaxed or not. Gronke et al. (2014) refined the method to take into account the effects of modified gravity in the virialisation state of the halos.

In this paper, however, filtering the non-relaxed halos would eliminate too many halos in the extreme models, leaving almost none remaining. For this reason we neglect to filter the non-relaxed halos from the relaxed ones.

The halo profiles are calculated by binning dark matter particles and the baryonic gas properties in annular bins for each halo, then averaging over all halos. We focus only on the present day epoch which corresponds to

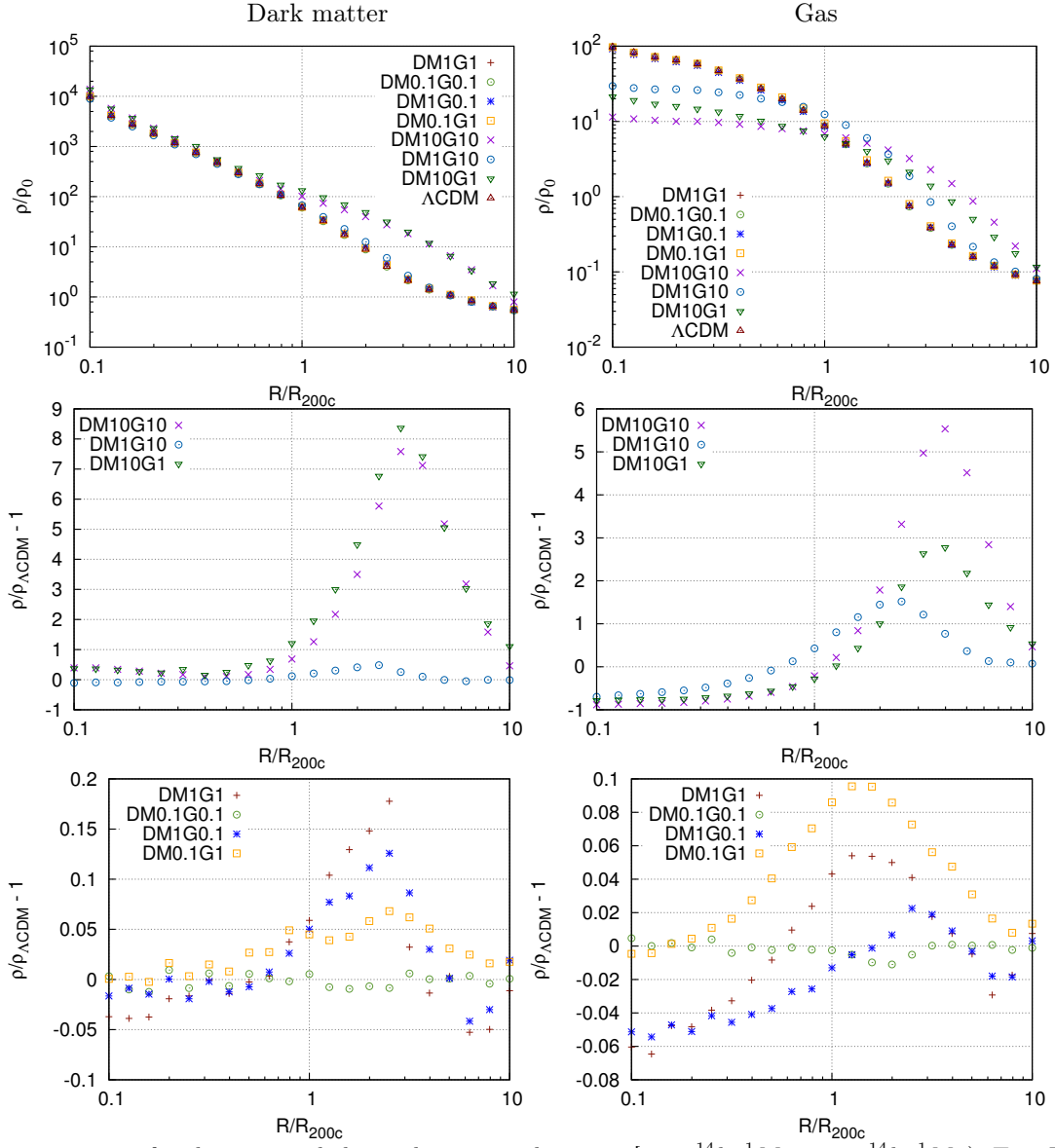


Fig. 3. Density properties for the massive halos with mass in the range $[1 \times 10^{14} h^{-1} M_{\odot}, 5 \times 10^{14} h^{-1} M_{\odot}]$. Top: Density profiles for Λ CDM and the symmetron models. Middle: Density profile deviations from Λ CDM for the extreme models. Bottom: Density profile deviations from Λ CDM for the remaining models. Left column show the dark matter component, while the right column show the gas component.

$z = 0$. The profiles range from 10% of the virialisation radius, $r = 0.1R_{200c}$, to ten times the virialisation radius, $r = 10R_{200c}$. This range was chosen to properly catch all behaviours of the fifth-force on the dark matter and gas halos while also avoiding the inner regions of the halos where the resolution of our simulations is low.

5.1. Massive halo set density profiles

The density halo properties for massive, potentially fully-screened, halos are presented in Fig. 3. An extreme coupling in the dark matter will strongly affect both the dark matter and gas density profiles. For the dark matter profiles the effect is mostly contained at the exterior of the dark matter halos, while the gas profiles show signs of the extreme dark matter coupling in all parts of the halo and outside. The diminished clustering at the inner regions of the halos

can be explained by an environmental effect from the dark matter on the gas.

The dark matter will cluster faster than the gas due to its collisionless nature, where the gas gets prevented from collapsing due to the pressure etc. the dark matter will cluster unhindered. This means that the dark matter will reach higher densities at a faster rate than the gas, and from the description of the screening mechanism we know that the screening is triggered by a combined density, dark matter plus gas, threshold, resulting in the dark matter triggering the screening mechanism before the scalar field has had a chance to work on the gas component as much as on the dark matter.

An extremely coupled gas has a minor, however not negligible, effect on the dark matter profiles while a huge impact on the gas profiles. This is expected as there is much more dark matter than gas, resulting in the effect of the gas not being as strong. Note also that 10G10 is the model

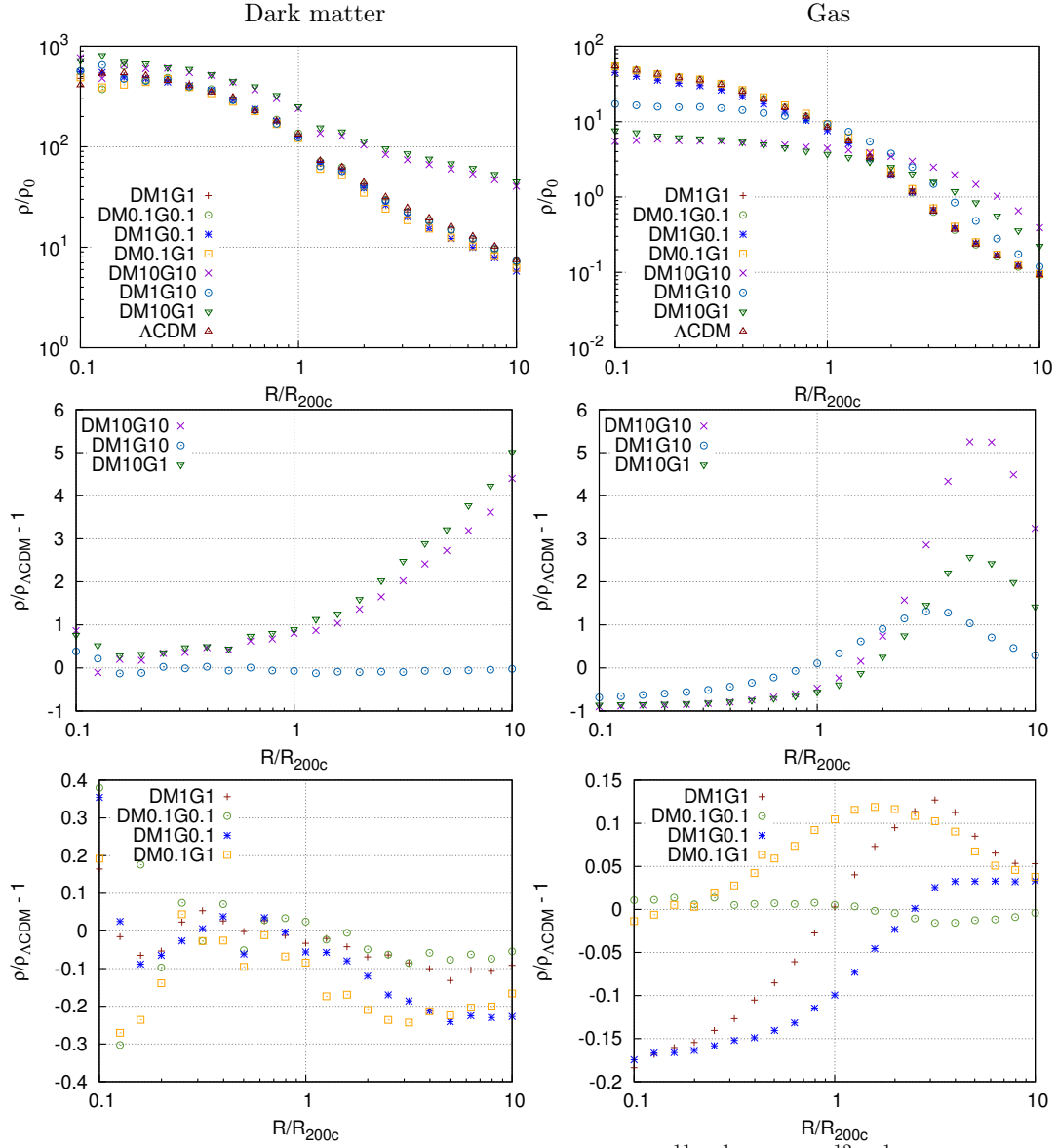


Fig. 4. Density properties for the small halos with mass in the range $[5 \times 10^{11} h^{-1} M_{\odot}, 1 \times 10^{12} h^{-1} M_{\odot}]$. Top: Density profiles for Λ CDM and the symmetron models. Middle: Density profile deviations from Λ CDM for the extreme models. Bottom: Density profile deviations from Λ CDM for the remaining models. Left column show the dark matter component, while the right column show the gas component.

with the biggest effects on the gas profiles, while the dark matter profiles seem to prefer DM10G1.

5.1.1. Small halo set density profiles

Studying the small, most likely non-screened, halo set density profiles in Fig. 4 reveal similar density profiles as for the massive halos, however the scalar field has a larger impact on these density profiles, particularly in the outer regions of our profiles. From 10G10 and DM10G1 we can see that the gas profiles for the small halos are highly dependent on the dark matter coupling in the inner regions of the halo, so much so that the coupling to the gas is almost negligible, outside of the halo however we note that the gas coupling starts to distinguish DM10G1 from 10G10.

5.2. Density profiles deviations

The deviations from Λ CDM for the massive halo set are found in the lower two rows of Fig. 3. The deviations confirm the conclusions from the total density profiles, and also reveal previously unseen effects. All models without an extremely coupled dark matter (10G10 and DM10G1) makes the dark matter halos cluster less at the inner regions than in those two cases. The exact opposite occur in the gas power spectra, where all the extremely coupled models (the two previously mentioned and DM1G10) cluster less than the other models. This is due to the baryonic physics preventing the gas from collapsing as far inwards as the dark matter, and then the gravitational contribution from the gas on the dark matter also prevents the dark matter from clustering.

The peak of deviations does not occur at the same radius for all the models. For DM1G10 the peak in deviations is closer to the halo centre, while for 10G10 and DM10G1

the deviations peak further out. This effect is due to the extreme coupling in the gas. The extreme coupling allow the scalar field to affect the gas component to such an extent that it collapses further inwards before the environmental effect of the combined density triggers the screening mechanism.

The bottom row reveal that DM1G10 has a strong effect on the dark matter halos throughout the entire density profiles, with higher peak deviation than DM1G1. The gas profiles are under-dense at the inner regions of the halos in the cases where the dark matter is normally (or extremely) coupled to the scalar field, in the cases where the dark matter is minimally coupled the profiles approach Λ CDM at the centre of the halos. This behaviour further asserts our conclusions about the environmental effect.

5.2.1. Small halo set profiles deviations

The deviation profiles for the small halos are presented in the middle and bottom row of Fig. 4. In the small halos the deviations are not oscillating around the Λ CDM value as they do in the massive halos, the effect of the scalar field is found throughout the halos and beyond. With the exception of the extreme models the small halos show a stronger deviation from Λ CDM in the dark matter density profiles. Comparing 10G10, DM1G10 and DM10G1 between the halo sets show that the small halos differ a lot more from the massive halos in the dark matter profiles than in the gas profiles, while the other less coupled models show significant differences in both the gas and dark matter profiles.

To study how deviations from Λ CDM differ in the dark matter and gas cases we introduce the “deviation bias” δ^{DM} defined as the relative difference between the deviations

$$\delta^{DM} = \left| \frac{\Delta_{DM} - \Delta_{Gas}}{\Delta_{Gas}} \right| = \left| \frac{\frac{\rho_{DM} - \rho_{\Lambda CDM}}{\rho_{\Lambda CDM}} - \frac{\rho_{Gas} - \rho_{\Lambda CDM}}{\rho_{\Lambda CDM}}}{\frac{\rho_{Gas} - \rho_{\Lambda CDM}}{\rho_{\Lambda CDM}}} \right|.$$

The massive halo set DM10G1 model represents a model that has an enormous deviation from Λ CDM in the dark matter component of $\Delta_{DM} \sim 8.5$ at $R \sim 4R_{200c}$ while having a much smaller deviation of $\Delta_{HB} \sim 2.5$ in the gas component, giving a deviation bias of $\delta^{DM} \approx 2.4$. The same effect, working the other way around, is present in DM1G10 where the deviations from Λ CDM are $\Delta_{HB} \sim 1.5$ for the gas and $\Delta_{DM} \sim 0.5$ for the dark matter, giving a deviation ratio of $\delta^{DM} \approx \frac{2}{3}$. This effect is also clearly visible in the small halo set.

5.2.2. Bias from density profiles

One of the aims of this paper is to find a method of distinguishing between models that have universal coupling and models with non-universal coupling. For this purpose we introduce the density bias

$$b_d = \frac{\rho_{DM}}{\rho_{gas}}, \quad (27)$$

as presented in Fig. 5 for the massive halos and Fig. 6 for the small halos.

The massive halo density bias show that all the models have the same behaviour as Λ CDM, except the three models 10G10, DM1G10 and DM10G1. 10G10 converges with the Λ CDM bias earlier than DM1G10 and DM10G1, however in general has a higher deviation at the inner region.

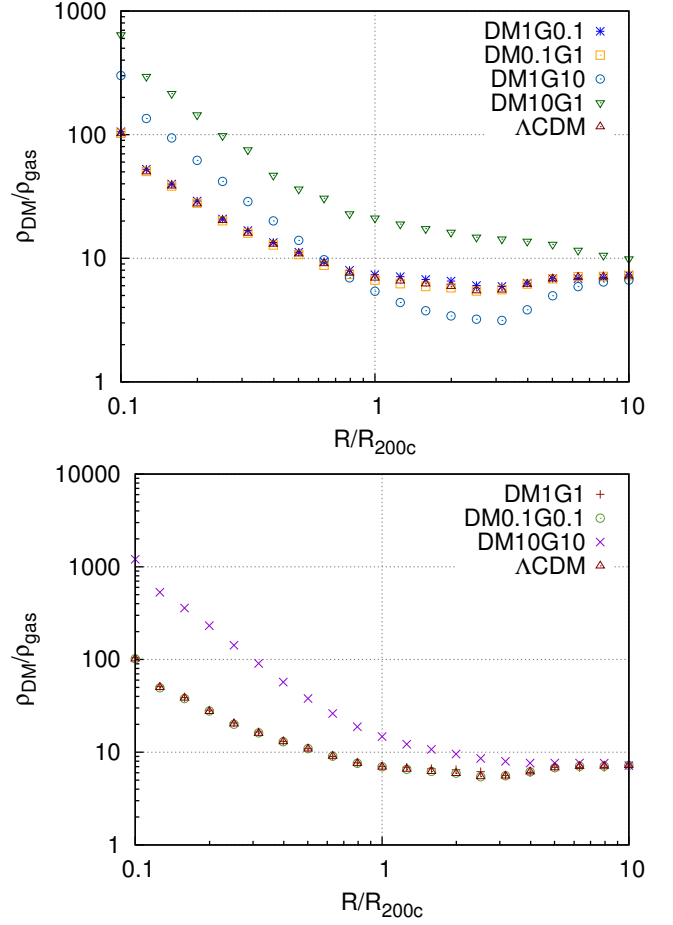


Fig. 5. Density bias for the massive halo set. Top: Models with non-universal coupling. Bottom: Models with universal coupling.

The small halo density bias show a completely different behaviour in general. Studying DM1G1, DM0.1G0.1, DM1G0.1 and DM0.1G1 reveals that the models with a universal coupling seem to deviate less from Λ CDM than the models with a non-universal coupling. The same behaviour can be seen in the massive halo set as well.

This is the same behaviour we noticed for the power spectrum bias at larger scales, and allows us to conclude that significant deviations in the density bias from the Λ CDM model throughout the halos might be an indication of a non-universal coupling.

5.3. Temperature

The temperature is a very interesting component to study due to its close relation observables (Wilcox et al. 2015; Terukina et al. 2014). The temperature is not an output of our code and needs to be reconstructed using the ideal gas law,

$$p = R_s \rho T, \quad (28)$$

where p is the thermal pressure, $R_s = \frac{k_B}{m_H}$ is the specific gas constant and ρ is the gas density. The temperature profiles are made and analysed in the exact same way as the density profiles.

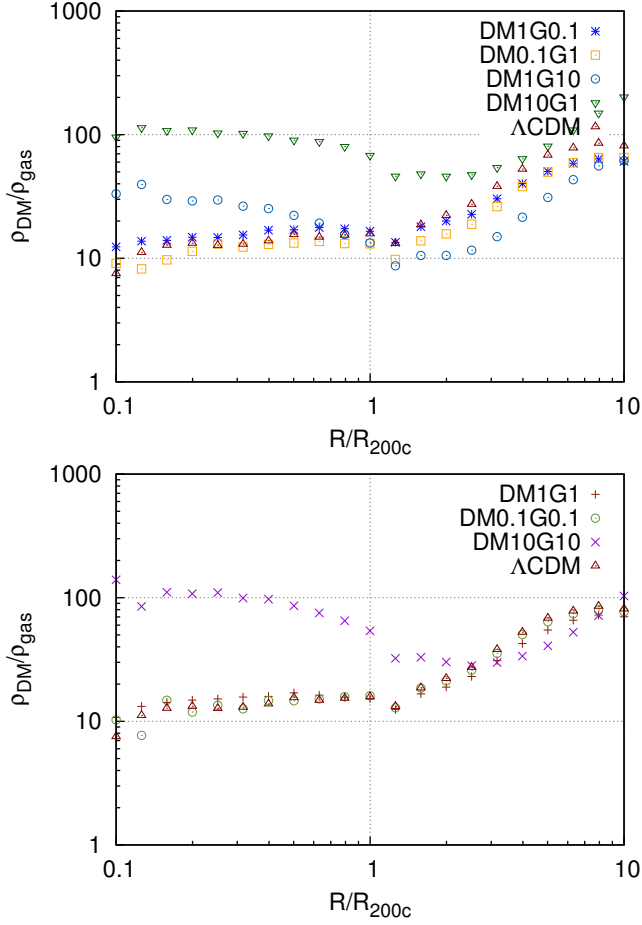


Fig. 6. Density bias for the small halo set. Top: Models with non-universal coupling. Bottom: Models with universal coupling.

5.3.1. Total temperature profiles

The temperature profiles are presented in Fig. 7. The temperature is a product of the baryonic processes and is most sensitive to strong coupling between the gas and the scalar field (Hammami et al. 2015).

The stronger the coupling to the scalar field is, the higher the temperature in the halos is. The slope of the profiles outside of the halo, as the temperature starts dropping, is shallower for 10G10, DM1G10 and DM10G1 than in the other models. Note that 10G10 gives an even higher temperature than DM1G10, telling us that the dark matter plays a vital role in the temperature of the baryonic halos. This is also evident from DM10G1 that has a higher temperature than the less extreme cases.

The small halos show in general less of a slope throughout the halos, particularly at the very outer regions where the temperature started plummeting in the massive halos.

5.3.2. Temperature profiles deviations

The temperature deviations from the Λ CDM temperature are found in the bottom two rows of Fig. 7 and Fig. 8 for the massive and small halo sets respectively.

DM0.1G1 and DM0.1G0.1, two similar models where one has universal coupling and the other does not, display no signatures that can be interpreted as a trait of non-universal coupling. DM1G0.1 and DM0.1G0.1 on the other

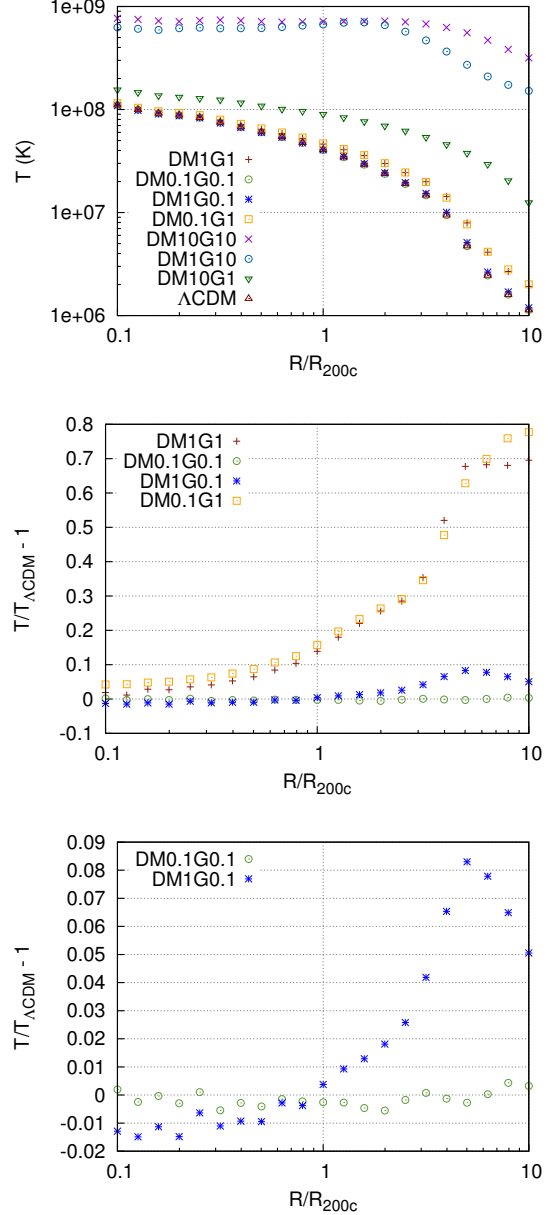


Fig. 7. Temperature properties for the massive halos. Top: Temperature profiles for Λ CDM and the symmetron models. Middle: Temperature profile deviations from Λ CDM. Bottom: Deviations with the extremely coupled models filtered out.

hand display an increase in temperature outside of the virialisation radius.

These effects both come from the fact that these halos are so massive that they are most likely screened from the scalar field. The difference between DM1G0.1 and DM0.1G0.1 is due to the regions outside of the halos being non-screened, and the extreme coupling to the dark matter allows it to get influenced by the scalar field to a larger extent than the other model.

5.3.3. Small halo temperature profiles deviations

The small halos have vastly different characteristics. Studying DM1G0.1 and DM0.1G0.1 again show that while DM0.1G0.1 fluctuates around the Λ CDM value, as is to

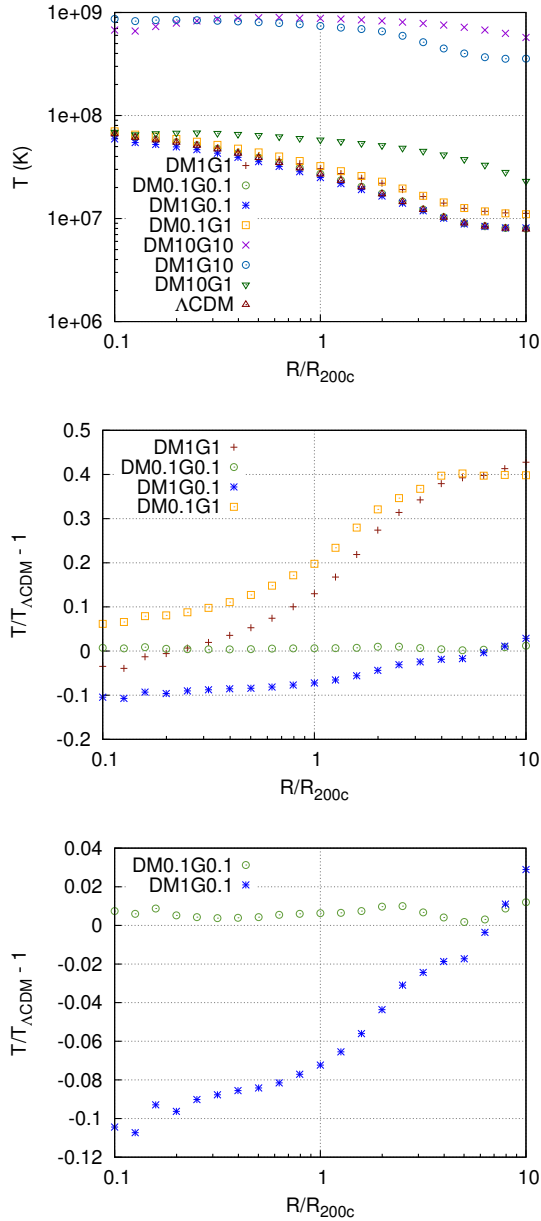


Fig. 8. Temperature properties for the small halos. Top: Temperature profiles for Λ CDM and the symmetron models. Middle: Temperature profile deviations from Λ CDM. Bottom: Deviations with the extremely coupled models filtered out.

be expected, DM1G0.1 starts far below the Λ CDM value and steadily climbs. Almost the exact same behaviour is present between DM0.1G1 and DM1G1. The model with an extreme dark matter coupling has a lower temperature through most of the halo.

The effects of coupling the dark matter to the scalar field stronger than the gas will lower the temperature, counter to what we would conclude from comparing DM10G1 to DM1G1, however, it stands to reason that the higher temperatures in DM10G1 comes from the extreme coupling, and not due to the non-universal coupling. In general the temperature of the halos are first and foremost dependent on the gas coupling, unless dealing with extreme coupling values.

6. Conclusions

In this paper we investigate scalar-tensor theories of gravity which present a non-universal coupling. That is, baryons and dark matter are coupled to the scalar degree of freedom with different coupling strengths. The models we investigate utilises a screening mechanism to suppress the deviations from General Relativity at small (Solar System) and large cosmological scales. Specifically, the symmetron screening mechanism.

Due to the screening mechanism, the strongest signatures in these models are expected to occur at the non-linear regime of structure formation. Therefore, in order to unveil the imprints of such theories at astrophysical scales, we have run several hydrodynamic cosmological N-body simulations. We have compared models with and without a universal coupling to the symmetron scalar field, and have shown that several astrophysical observables (density profiles, temperature profiles and power spectra) show significant differences between the dark matter and gas components when the coupling is non-universal.

The density profiles show that deviations from Λ CDM can vary significantly between the gas and dark matter, in the same model with the same cosmology, mostly with the dark matter having larger deviations from Λ CDM than the gas, sometimes with several factors of difference. This results from the fact that dark matter largely dominates over baryons at those scales. Therefore, the impact of a dark matter component strongly coupled to the scalar field is quite important.

We have also demonstrated the efficiency of the symmetron screening mechanism exceptionally well by studying the temperature profile deviations in large, massive halos and in small, less massive halos. As is common in screened modified gravity theories, the effects are larger in smaller halos where the density is too low for the force to be screened; while in large massive halos the fifth force from the scalar field is strongly suppressed, therefore minimally affecting the physical observables.

Attempting to find signatures in the density profiles and power spectra that would reveal to us whether the coupling to the scalar field is universal or not revealed one signature: in the cases of universal coupling the deviations in the bias from Λ CDM is smaller than in the cases of non-universal couplings throughout the halos. This is expected, since General Relativity is a universally coupled theory. If observers find the density profile bias or power spectrum bias to deviate from the calculated Λ CDM bias then this might very well be a sign of a non-universal coupling, and therefore a breaking of the equivalence principle.

Separating the dark matter and gas will prove a challenge for observers since the dark matter is not a direct observable, while the gas is, particularly with the intent of comparing to theories. To work around this we propose to use the density bias presented in this paper. To measure this density bias we suggest to first construct the total density profile, $\rho_{Tot} = \rho_{DM} + \rho_{gas}$, by using velocity profiles which would mainly be dependent on the mass within, then construct the gas density profile ρ_{gas} by using temperature profiles.

If one takes seriously the possibility of matter components with a non-universal coupling to a gravity scalar degree of freedom, then our work shows the bias will be greatly affected. Therefore, attempts to rule out or constrain mod-

ified gravity theories by comparing dark matter predictions to the observed quantities based on baryonic properties may be misleading, and one must consider the possibility of a non-universal coupling that might skew the conclusions and the dark matter properties which are inferred from baryons.

7. Acknowledgements

The authors thank C. Llinares and H. Winther for sharing the ISIS code to run the simulations performed in this article. We also thank M. Grönke and H. Winther for comments and suggestions. The authors thank The Research Council of Norway for funding and the NOTUR facilities for the Computational resources.

References

- Barreira, A., Li, B., Hellwing, W. A., Baugh, C. M., & Pascoli, S. 2013, JCAP, 1310, 027
- Barrow, J. D. & Mota, D. F. 2003, Class.Quant.Grav., 20, 2045
- Behroozi, P. S., Wechsler, R. H., & Wu, H.-Y. 2013, ApJ, 762, 109
- Bertotti, B., Iess, L., & Tortora, P. 2003, Nature, 425, 374
- Boehmer, C. G. & Mota, D. F. 2008, Phys.Lett., B663, 168
- Brans, C. & Dicke, R. H. 1961, Physical Review, 124, 925
- Brax, P., Davis, A.-C., Li, B., & Winther, H. A. 2012, Phys. Rev. D, 86, 044015
- Brax, P., Davis, A.-C., Li, B., Winther, H. A., & Zhao, G.-B. 2013, J. Cosmology Astropart. Phys., 4, 29
- Brown, I. A. & Hammami, A. 2012, J. Cosmology Astropart. Phys., 4, 2
- Clifton, T., Ferreira, P. G., Padilla, A., & Skordis, C. 2012, Phys. Rep., 513, 1
- Colombi, S. & Novikov, D. 2011, POWMES: Measuring the Power Spectrum in an N-body Simulation, astrophysics Source Code Library
- Davis, A.-C., Li, B., Mota, D. F., & Winther, H. A. 2012, Astrophys.J., 748, 61
- de Felice, A. & Tsujikawa, S. 2010, Living Reviews in Relativity, 13, 3
- Dimopoulos, S., Graham, P. W., Hogan, J. M., & Kasevich, M. A. 2007, Physical Review Letters, 98, 111102
- Faraoni, V., Gunzig, E., & Nardone, P. 1999, Fund. Cosmic Phys., 20, 121
- Fujii, Y. & Maeda, K.-i. 2003, Classical and Quantum Gravity, 20, 4503
- Gronke, M. B., Llinares, C., & Mota, D. F. 2014, A&A, 562, A9
- Hammami, A., Llinares, C., Mota, D. F., & Winther, H. A. 2015, MNRAS, 449, 3635
- Hinterbichler, K. & Khoury, J. 2010, Phys. Rev. Lett., 104, 231301
- Hoyle, C. D., Kapner, D. J., Heckel, B. R., et al. 2004, Phys. Rev. D, 70, 042004
- Khoury, J. 2010, ArXiv e-prints [arXiv:1011.5909]
- Khoury, J. & Weltman, A. 2004, Phys. Rev. D, 69, 044026
- Koivisto, T. S., Mota, D. F., & Zumalacarregui, M. 2012, Phys.Rev.Lett., 109, 241102
- Li, B., Mota, D. F., & Barrow, J. D. 2011, Astrophys.J., 728, 109
- Li, B., Zhao, G.-B., Teyssier, R., & Koyama, K. 2012, J. Cosmology Astropart. Phys., 1, 51
- Llinares, C. & Mota, D. F. 2013, Physical Review Letters, 110, 161101
- Llinares, C. & Mota, D. F. 2014, Phys. Rev. D, 89, 084023
- Llinares, C., Mota, D. F., & Winther, H. A. 2014, A&A, 562, A78
- Martel, H. & Shapiro, P. R. 1998, MNRAS, 297, 467
- Misner, C. W., Thorne, K. S., & Wheeler, J. A. 1973, Gravitation
- Mota, D. F., Shaw, D. J., & Silk, J. 2008, Astrophys.J., 675, 29
- Neto, A. F., Gao, L., Bett, P., et al. 2007, MNRAS, 381, 1450
- Noller, J., von Braun-Bates, F., & Ferreira, P. G. 2014, Phys. Rev. D, 89, 023521
- Planck Collaboration, Ade, P. A. R., Aghanim, N., et al. 2015, ArXiv e-prints [arXiv:1502.01589]
- Puchwein, E., Baldi, M., & Springel, V. 2013, MNRAS, 436, 348
- Riess, A. G., Filippenko, A. V., Challis, P., et al. 1998, AJ, 116, 1009
- Schaller, M., Robertson, A., Massey, R., Bower, R. G., & Eke, V. R. 2015, ArXiv e-prints [arXiv:1505.05470]
- Shaw, L. D., Weller, J., Ostriker, J. P., & Bode, P. 2006, ApJ, 646, 815
- Sotiriou, T. P. 2006, Classical and Quantum Gravity, 23, 5117
- Terukina, A., Lombriser, L., Yamamoto, K., et al. 2014, J. Cosmology Astropart. Phys., 4, 13
- Vainshtein, A. I. 1972, Physics Letters B, 39, 393
- Wilcox, H., Bacon, D., Nichol, R. C., et al. 2015, ArXiv e-prints [arXiv:1504.03937]
- Will, C. M. 2014, Living Reviews in Relativity, 17, 4
- Winther, H. A., Mota, D. F., & Li, B. 2012, ApJ, 756, 166